12th International Symposium on Turbulence and Shear Flow Phenomena (TSFP12)
Osaka, Japan (Online), July 19-22, 2022

DIRECTED PERCOLATION PHENOMENA IN SUBCRITICAL TRANSITION OF HIGH-ASPECT-RATIO DUCT FLOW

Kazuki Kohyama
Department of Mechanical Engineering
Tokyo University of Science
2641 Yamazaki, Noda-shi, Chiba, 278-8510, Japan
7521701@ed.tus.ac.jp

Masaki Sano
Institute of Natural Sciences, School of Physics and Astronomy
Shanghai Jiao Tong University
800 Dongchuan RD. Minhang District, Shanghai, 200240, China
sano.masaki@sjtu.edu.cn

Keiichi Tamai
Research Center for Computational Design
of Advanced Functional Materials
National Institute of Advanced Industrial Science and Technology
1-1-1 Umezono, Tsukuba, Ibaraki, 305-8568, Japan
k-tamai@aist.go.jp

Takahiro Tsukahara
Department of Mechanical Engineering
Tokyo University of Science
2641 Yamazaki, Noda-shi, Chiba, 278-8510, Japan
tsuka@rs.tus.ac.jp

ABSTRACT

Directed percolation (DP) and subcritical turbulent transitions in channel flow, which have been a debatable issue in recent years, are investigated by direct numerical simulations for high-aspect-ratio channel flows with spanwise sidewalls, *i.e.*, very thin, wide duct flows. The presence of sidewalls in the duct flow prevented sustained stable localized turbulence band at low Reynolds numbers ($700 \lesssim Re \lesssim 1000$), which allowed global turbulence maintenance in the infinitely wide channel flow, and the critical values were approximately $Re_c = 1000$. Localized turbulence was spatio-temporally intermittency, and its split and decay were generally similar to those in the channel flow, although there were some behaviors specific to the duct flow. Long-term Lagrangian observation of the split and decay of localized turbulence near the criticality showed the branching of turbulence in the space-time-diagrams. The spatial dimension of the branching depended on the duct geometry, with a spatial one-dimensional spread when the distance between sidewalls was not wide enough (like in a square duct), but two-dimensional when it was wide, qualitatively confirming $(1+1)$-dimensional and $(2+1)$-D DP characteristics, respectively. The power-law scaling exponents for the Reynolds number dependence of the transition profiles were found to be consistent with the specific critical exponents of the two types of DPs, respectively.

INTRODUCTION

Wall-bounded shear flow in subcritical regime forms a large-scale intermittency of coexisting laminar and turbulent flow, even when the Reynolds number Re is much lower than the upper critical value Re_L determined by the linear stability. Also, once the flow becomes completely laminar, turbulence does not spontaneously nucleate, which is know as an absorbing phase transition. That is turbulence can be sustained globally by maintaining equilibrium localized structures. The localized turbulence generally has a large-scale spatio-temporal intermittency (STI). This phenomenon has been found to be universal at the onset of the subcritical turbulent transition. A well-known example is the turbulent puff in pipe flow, where laminar and turbulent regions are arranged alternately and intermittently with randomness only in the streamwise direction. Each turbulent puff may split into two turbulent puffs or decay and, as the Reynolds number goes down to the global-stability criticality, those two events are stochastically comparable (Avila *et al.*, 2011; Mukund & Hof, 2018).

Recently, these turbulent branching and some statistics of STI were shown to have directed percolation (DP) universality, as conjectured by Pomeau (1986). A narrow Taylor-Couette flow (TCf) and a wide-gap annular flow exhibit similar (1+1)-dimensional STI of pipe flow and follow $(1+1)$-D DP universality class, where the first number is the spatial dimension and the latter indicates time (Lemoult *et al.*, 2016; Takeda *et al.*, 2020). In other canonical flows in wide channels, the STI is more complicated because a spatially two-dimensional pattern is formed with turbulent stripe and oblique band (Prigent *et al.*, 2002; Barkley & Tuckerman, 2005; Tsukahara *et al.*, 2005; Duguet *et al.*, 2010; Tuckerman & Barkley, 2011; Tuckerman *et al.*, 2020). Some subcritical transitions in the wide channels were found to follow $(2+1)$-D DP universality class; the Waleffe flow by Chantry *et al.* (2016), the wide TCf by Klotz *et al.* (2022), and the channel flow (also known as plane Poiseuille flow, PPF) by Sano & Tamai (2016); Takeda & Tsukahara (2019); Shimizu & Manneville (2019).

For the PPF between two parallel infinite plates, the localized turbulence forms the stripe pattern consisting of oblique bands for $Re < 1500$ (Tsukahara *et al.*, 2010), despite the linear stability analysis by Orszag (1971) saying that $Re_L = 5772.2$. The experimental nominal-channel flow and the numerical PPFs with large-scale domains show good agreements with $(2+1)$-D DP universality class, but the transition profiles below the criticality ($Re < 1000$) deviates from that, where the flow can maintain turbulence for $Re \approx 800$ with isolated band which is (1+1)-D STI and straight ahead at an angle of approximately 45° (Tao *et al.*, 2018; Xiao *et al.*, 2021). The presence of spanwise sidewalls, *i.e.*, a duct as experimental channel, affects the intermittency formation. This sidewall and finite-size effects depend on the duct geometry such as the aspect ratio A defined in the flow-cross-section as a ratio of the long side against the short one. In a square duct of $A = 1$, $(1+1)$-D STI

Table 1. Computational conditions of medium- to high-aspect-ratio duct and plane Poiseuille flows (PPF). Case shows an aspect ratio of duct channels A ($\equiv L_z/L_y$), but $A\infty$ indicates the infinite channel (PPF) with periodic boundary condition in spanwise direction. L_i^* is the domain size non-dimensionalized by the channel half width δ, and N_i is the number of grids. The wall-unit resolutions Δ^+ are values at $Re_\tau = 64$, but at $Re_\tau = 48$ for $A\infty$ with largest case.

Case	$L_x^* \times L_y^* \times L_z^*$	$N_x \times N_y \times N_z$	Re_τ	Δx^+	Δy^+	Δz^+
$A24$	$512 \times 2 \times 48$	$4096 \times 64 \times 1016$	46–110	8.0	0.2–4.6	3.0
$A96$	$512 \times 2 \times 192$	$4096 \times 64 \times 4088$				
$A\infty$	$512 \times 2 \times 409.6$	$4096 \times 64 \times 4096$	49–110	8.0	0.2–4.6	6.4
	$819.2 \times 2 \times 1024$	$4096 \times 64 \times 8192$	37–49	9.6	0.2–3.5	6.0

shows the same phenomena as a turbulent puff in a pipe flow (Khan *et al.*, 2021). At $A = 9$, Takeishi *et al.* (2015) identified two-dimensional zigzag pattern like a stripe structure. The infinite/finite size effect might be a main cause of the modulation in DP features and of the critical values discrepancy.

In the present study, we performed direct numerical simulations (DNSs) of medium-to-high-aspect-ratio duct flows, up to $A = 96$, and the PPF in subcritical regime at low Reynolds numbers, to discuss the sidewall effect on DP features in turbulent branching and the transition profiles.

NUMERICAL SET-UP AND METHODOLOGY

Geometry of Duct Flow

The duct flow is considered as the flow in the channel between two parallel planes with two parallel sidewalls in the spanwise direction to be driven by a constant pressure gradient ($\mathrm{d}P/\mathrm{d}x$) in the streamwise (x) direction. The typical configuration is depicted in Fig. 1 with the three-dimensional Cartesian coordinates system. The geometry of the rectangular duct is determined by the distance between the spanwise sidewalls, that is, we used the width-to-height aspect ratio defined as

$$A \equiv \frac{L_z}{L_y} = \frac{L_z}{2\delta} \tag{1}$$

where δ is the channel half width in the wall-normal (y) direction. A typical example is the square duct flow with $A = 1$. A rectangular duct with $A > 1$ has a wider distance between the spanwise sidewalls, as shown in Fig. 1. In all cases, the streamwise velocity $u(y,z)$ is not uniform in the spanwise direction because of sidewalls and corners, unlike PPF. However, these effects attenuate for high-aspect-ratio. The detailed solution is in Wu & Song (2022); Kohyama *et al.* (under review).

In the present DNS study, we chose two different values of $A = 24$ and 96 to cover medium- and high-aspect-ratios. This range allows us to exhaustively investigate the sidewall effects on the turbulent flow and spatio-temporal intermittent structures. For reference, previous experimental nominal-channel (duct) flows in the subcritical region have been performed comprehensively with a wide range of aspect ratios $A = 7.5$ by Lemoult *et al.* (2012), 52 by Seki & Matsubara (2012), 83 by Yimprasert *et al.* (2021), 180 by Sano & Tamai (2016), and 245 by Paranjape (2019). However, since their the streamwise domain is finite, it has been difficult to discuss statistical steady states about their transition profiles and turbulent branching near the criticality. Except for the report of $Re_g = 1500$ for a narrow duct with $A = 7.5$ (Lemoult *et al.*, 2012), many experiments reported $Re_g \approx 1000$ or less for large values of A. Numerical studies have already confirmed a similar trend only for duct flows with low- to medium-aspect-ratios ($A = 1$–9, 50), but not for higher one (Khan *et al.*, 2021; Takeishi *et al.*, 2015; Wu & Song, 2022).

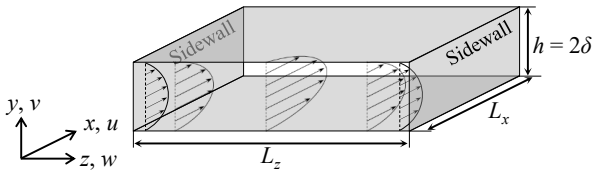

Figure 1. Schematic of rectangular duct flow. Boundary geometry is defined by the aspect ratio $A \equiv L_z/L_y\ (= L_z/2\delta) > 1$.

Computations

The non-dimensional governing equations for the velocity $u_i = (u, v, w)$ and the pressure p are the equation of continuity and the Navier–Stokes equation for incompressible Newtonian fluid in the Cartesian coordinate system $x_i = (x,\ y,\ z)$:

$$\frac{\partial u_i^+}{\partial x_i^*} = 0 \tag{2}$$

$$\frac{\partial u_i^+}{\partial t^*} + u_j^+ \frac{\partial u_i^+}{\partial x_j^*} = -\frac{\partial p^+}{\partial x_i^*} + \frac{1}{Re_\tau}\frac{\partial^2 u_i^+}{\partial x_j^{*2}} + f_i \tag{3}$$

where the superscripts of * and $^+$ indicate quantities non-dimensionalized by δ and the friction velocity u_τ, respectively. f_i in the last term of Equation (3) is a body force to mimic the sidewall solid phase in the channel flow by means of the immersed boundary method (IBM). The control parameter of the present DNS is the friction Reynolds number Re_τ normalized by u_τ converted from the constant pressure gradient: $Re_\tau \equiv \delta u_\tau/\nu = \delta\sqrt{-\mathrm{d}P/\mathrm{d}x^*}/\nu$. Here, the pressure P is already divided by the fluid density ρ, and ν represents the kinematic viscosity. Given a sufficiently large A, the friction velocity asymptotically approaches $u_\tau = \sqrt{\tau_{\mathrm{w},y}/\rho}$ with the wall shear stress $\tau_{\mathrm{w},y}$ on the main wall surface at $y = 0$ and 2δ. In the following discussion, we use the Reynolds number Re defined with the streamwise velocity at the center line in laminar flow $u_{\mathrm{c\ lam.}} = u_\tau Re_\tau/2$ as

$$Re \equiv \frac{\delta u_{\mathrm{c\ lam.}}}{\nu} = Re_\tau^2/2 \tag{4}$$

We adopted two types of numerical boundary conditions: the non-slip and the periodic boundary conditions. The non-slip condition was adopted on the main walls normal to the y direction, while the periodic boundary conditions were in the x direction. The non-slip boundary on the spanwise sidewall was configured by the direct-forcing IBM around the spanwise end faces of the computational domain (Fadlun *et al.*, 2000). We applied the following IBM rules to the staggered-grid velocity components at the sidewall boundary: no inflow or outflow at the sidewall surfaces, and $\mathbf{u} = \mathbf{0}$ inside the sidewalls.

Equations (2) and (3) were spatially discretized using finite differences and with fine enough grid resolutions Δx_i^+, as listed in Table 1, according to the standard criteria of DNSs (Tsukahara *et al.*, 2005). We adopted the uniform grid in the x

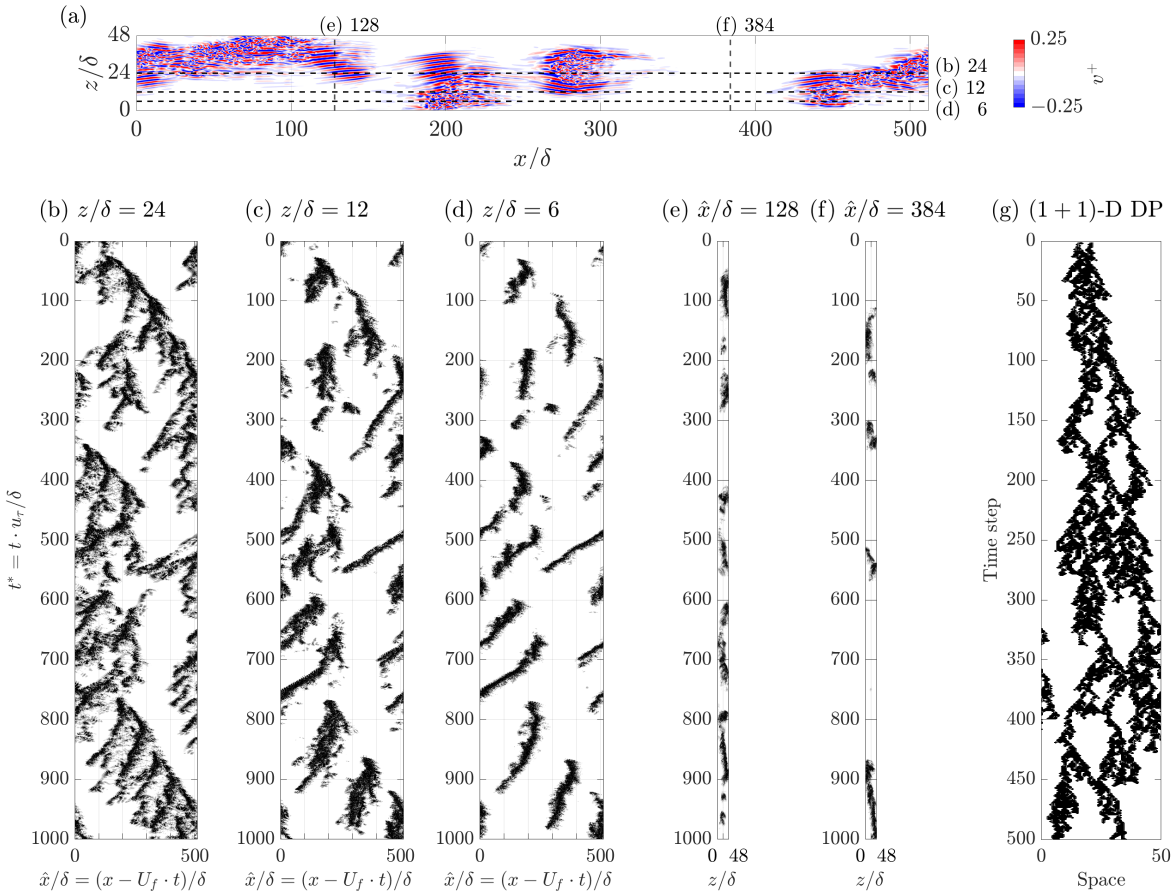

Figure 2. Typical instantaneous flow field and space-time-diagrams (STDs) in duct flow with $A24$ for $Re = 1128$. (a) Snapshot of instantaneous intermittency with turbulent spots and oblique bands visualized by the wall-normal velocity v^+ in the channel central x–z plane at $y = \delta$. The sidewalls are at $z/\delta = 0$ and 48. (b–f) STDs of $|v^+(\hat{x}$ or $z,\ t)|$ as the spatio-temporal intermittencies which indicate localized turbulence blanching. Localized turbulences are shown in black and laminar flow in white. In (b,c,d), spaces are the streamwise direction at near the sidewall to the center between the sidewalls as on the dashed lines $z/\delta = 6$, 12 and 24 in (a). Here, the space $\hat{x}$ $(= x - U_f \cdot t)$ is in Lagrangian coordinate corrected with the frame speed $U_f = 15.5u_\tau$. In (e,f), space is taken in the spanwise direction at $\hat{x}/\delta = 128$ and 384. (g) typical STD of $(1+1)$-dimensional directed site percolation (DP).

and z directions and the non-uniform in y, where the grid was finer near the main wall, cited from Moin & Kim (1982). For the present DNS of duct flows, the spanwise grid sizes were finer than those for PPF, especially because of the boundary layer on the spanwise sidewalls. Table 1 lists the parameters for the rectangular duct flows and the PPF. The time advancement was carried out using the second-order Crank–Nicolson and Adams–Bashforth schemes for the viscous term in the y direction and the other terms, respectively. Further details about the numerical methods used can be found in Abe *et al.* (2001).

RESULTS AND DISCUSSIONS

We discuss the spatial spread of the spliting and decaying behavior of localized turbulence in duct flows with the $A = 24$ and 96 from the space-time-diagrams (STDs). Its dependence on the distances from the sidewall surface and the aspect ratio are also discussed. Subsequently, based on the DP scaling theory, the critical exponents of the transition profiles such as the Reynolds number dependence of the turbulent fraction that follow a power law near the criticality are assessed in reference to the unique exponent values of DP universality classes. For reference, DP scaling was also performed for that of the PPF. The differences from the duct flow in terms of the critical values, the exponents and its fitting range were investigated.

Spatio-Temporal Intermittency

Figure 2(a) and 3(a) show typical instantaneous flow fields in both ducts in the x–z plane at the mid-channel of $y = \delta$ near the criticality for different aspect ratios. High fluctuations of the wall-normal velocity v^+ in red and blue indicate longitudinal streaks and fine vortices as turbulence. To summarize briefly, the intermittencies depend on the spanwise domain size, as shown below. The duct flow with $A24$ does not form a perfect one-dimensional intermittency like a puff, but forms an quasi-1D structure in the streamwise direction consisting of turbulent spots and short oblique bands. For $A96$, the spot is not stationary, but some growing bands are dominant, and leads to a 2D structure similar in PPF. For the details of their stochastic behaviors, see Kohyama *et al.* (under review).

Localized turbulence is usually advected in the streamwise direction with bulk velocity u_m, since there is positive mean flow in the PPF and duct flow. STDs represent the time evolution of turbulent and laminar flows at the space marked by the dashed lines in Figs. 2(a) and 3(a) from a Lagrangian view. For example, the horizontal axes of STDs in Figs. 2(b-d) and 3(b-e) are the streamwise space, but observed from a Lagrangian coordinate (*i.e.*, $x \mapsto \hat{x} \equiv x - U_f \cdot t$). Here, the frame velocity U_f is slightly larger than the bulk velocity u_m in the critical neighborhood focused on in this study ($U_f > u_m \approx 14.5u_\tau$). Because a turbulent band's head grows

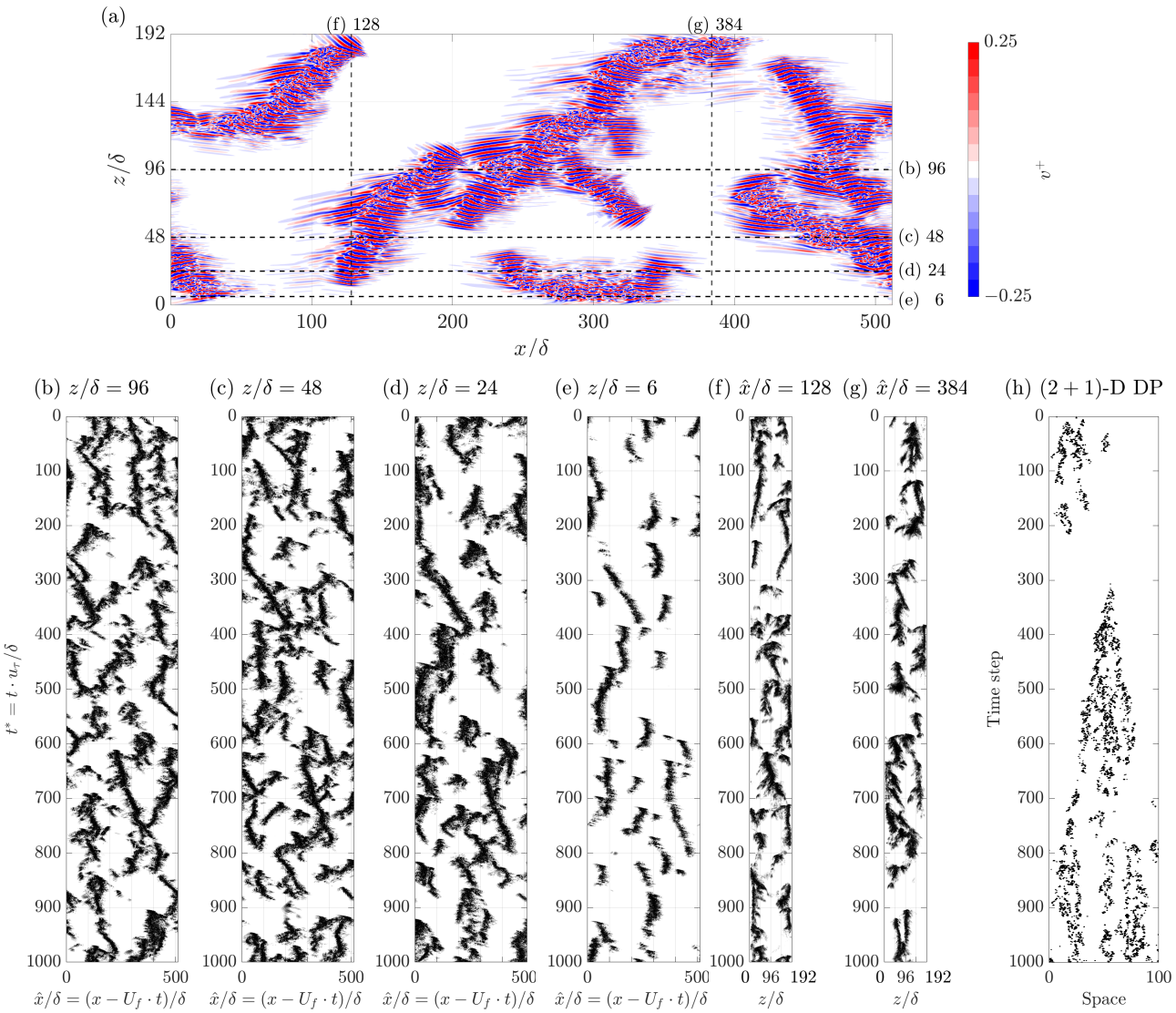

Figure 3. Typical instantaneous flow field and STDs in duct flow with $A96$ for $Re = 1105$. (b-g) STDs presented in the same manner as in Fig. 2, but the frame speed is $U_f = 15.25u_\tau$. (h) typical STD of $(2+1)$-D site DP for one spatial direction in the 2D space.

obliquely and extends to the downstream faster than u_m . Note, in the beginning of the intermittency away from the criticality, *e.g.*, when a robust stripe pattern is formed, U_f and u_m are approximately the same. For details of STD in a frame moving Lagrangian view, see Kashyap *et al.* (2020), but in the PPF.

Subsequently, the branching structure of the localized turbulence is compared with the STDs of $(1+1)$-D and $(2+1)$-D site DP shown in Figs. 2(g) and 3(h), respectively, which is one of the models of directed percolation. The details about the DP model can be found in Henkel *et al.* (2008). Then, we will qualitatively estimate the dependence on the distance from the sidewalls with respect to the presence or absence of DP-like features in the spatial spread of the branching.

For the STI of $|v^+(\hat{x},t)|$ in the narrow duct flow with $A24$, the STD at the center of the sidewalls ($z = 24\delta$) shown in Fig. 2(b) is in a good qualitative agreement with the STI of $(1+1)$-D DP shown as an example in Fig. 2(g). However, the STIs at $z = 6\delta$, 12δ near the sidewall shown in Fig. 2(c,d) do not have a single series of branches like the feature of $(1+1)$-D DP. The STDs of $|v^+(z,t)|$ in the span space shown in Fig. 2(c,d) are similarly strongly influenced by the sidewalls, each having only independent events: band and spot attachment, decay, and reflection at the sidewalls. It indicates that the DP phenomenon is not effective in the spanwise direction in cases where the domain is so narrow that turbulence does not split in the spanwise direction. As shown in Fig. 3(b,c), the both STDs at $z = 48\delta$ and 96δ as far away from the sidewall are qualitatively almost the same for the wide duct flow of A96, indicating that the sidewall effect is not significant. This branching is also two-dimensional based on the STDs in the spanwise direction at $\hat{x} = 128\delta$ and 384δ shown in Fig. 3(f,g). These branches are two-dimensional, which are different from Fig. 2(b), and qualitatively similar to the STD of $(2+1)$-D DP shown in Fig. 3(h), although slightly different. Closer to the sidewall ($z = 6\delta$ and 24δ), as shown in Fig. 3(d,e), the splitting behavior of the developed localized turbulence becomes weaker. Thus, STI is affected by the sidewalls and STD depends on its location, *i.e.*, it is actually not characterized by branching because of turbulence trapping on the sidewalls.

In summary, the stochastic behaviors of bands, including the splitting, colliding, and decaying, appear as a branching process, as illustrated in the STDs of localized turbulence. In Fig. 2(b), the duct flow of $A24$, which is strongly affected by the sidewall and the finite size effect, forms a spatially one-dimensional branching process similar to $(1+1)$-D DP STI, in spite of asymmetry in the streamwise direction. This is not true for $A96$ (Fig. 3(b,c)), where we should consider a spatially two-dimensional intermittency like in the infinite channel flow

(PPF). We may conjecture that DP universality changed from $(1+1)$-D to $(2+1)$-D between $A24$ and $A96$. On another note, to reproduce more exactly the STD such as asymmetry or fractal-like branching, it will be necessary to adopt the DP-based model proposed by Manneville & Shimizu (2020) or the Domany-Kinzel (DK) model, which generalized DP model.

Transition Profiles and Critical Exponents

The transition profile can be described as the Reynolds number dependency of the order parameter from a developed turbulence to fully-laminar state. For the order parameter which indicates the macroscopic order in the overall system, the turbulent fraction was adopted, which is the degree of spatial intermittency, *i.e.*, the fraction of localized turbulence in the total domain. The temporal turbulent fraction F_t was calculated using the wall-normal velocity in the x–z plane at the center of the main channel ($y=\delta$) as shown in Figs. 2(a) and 3(a), using the binarization of turbulent or laminar state with the threshold as $|v^+(x,\delta,z)|_\theta = 0.1$. Note that $F_t = 0$ corresponds to the fully-laminar, and $F_t \approx 1$ the fully-developed turbulent state. In the profiles, the turbulent fraction $\langle F_t \rangle_t$ is long-term-averaged over F_t at the statistical steady state (at least $500\delta/u_\tau$, *i.e.*, about 15 wash-out times in the streamwise domain), which is much longer than the time scale of the band-splitting frequency, even near the criticality. In particular, the time scale of the turbulence branching phenomenon becomes significantly longer as the critical value is approached, so the time-averaging is longer than $\Delta t^* = 1000$ in the vicinity of the critical value. Based on the transition profiles ($\langle F_t \rangle_t$ *vs.* Re) of two duct flows and the PPF, we investigated the presence or absence of DP universality class' scaling laws in power-like transition, their critical values and exponents, and the global critical Reynolds number Re_g, which is the lower bound for sustained turbulence. (Figure for profiles is not shown in this paper, but is available in Kohyama *et al.*, under review.)

Profiles of phase transitions are often followed by a power law of the control parameter (in this study, the Reynolds number). The present profiles in the near criticality similarly agree with the following power-law scaling as

$$\langle F_t \rangle_t \sim \left(\frac{Re - Re_c}{Re_c} \right)^\beta \tag{5}$$

where Re_c is the critical Reynolds number of profile following the power law and β is the critical exponent with positive value. The critical Reynolds numbers Re_c and the critical exponents β of the duct flows and the PPF transition profiles are summarized in Table 2, calculated by scaling according to Equation (5). The global critical values Re_g as cited from Kohyama *et al.* (under review) are also noted. In general, Re_c differs from Re_g due to the domain size effects: *e.g.*, $Re_c = 994$ and $Re_g = 722$ in the PPF of $A\infty$. However, in the present duct flows, the difference between the two critical values is not so significant, indicating a "pure" second-order phase transition.

In terms of the DP universality and the scaling theory, β in Equation (5) has a specific value depending on the spatial dimension of the intermittency. For example, if turbulent spots spread one-dimensionally, we expect $\beta_{(1+1)\text{-D}} \sim 0.276$, whereas $\beta_{(2+1)\text{-D}} \sim 0.583$ if two-dimensionally. The critical values for both the duct flow with $A96$ and the PPF corresponding to $A\infty$ were about $Re_c = 1000$, and both critical exponents agreed with $\beta_{(2+1)\text{-D}}$ within the error range. Also, the critical value for wide duct flow asymptotically approaches $Re_c \approx 1000$, which is consistent with the expectation in the nominal-channel flow experiment in Carlson *et al.* (1982) that three-dimensional disturbances grow to turbulence at $Re > 1000$. While, for the duct flow with $A24$, the critical value is slightly higher ($Re_c = 1119$), and the critical exponent is lower ($\beta = 0.28 \pm 0.02$) and in agreement with $\beta_{(1+1)\text{-D}}$, indicating a drastic transition to fully-laminar flow and sensitivity to changes in the Reynolds number around the criticality. Note, the large error range of the critical exponent in the PPF is due as the plots when the order parameter is close to $\langle F_t \rangle_t = 0$ are not near the critical value Re_c and not included in the fitting, which is due to the peculiar PPF profile. Due to the characteristic turbulence-maintaining structure at $700 \lesssim Re \lesssim 1000$ in PPF, the profile at $Re < 1155$ deviates from the second-order phase transition. Where, the fitting ranges are different, as shown in Table 2, but generally $1100 \lesssim Re \lesssim 1500$ as near the critical values. However, above this Reynolds number region, all profiles are the same and the curve becomes gradual and deviates from the critical exponent of DP. Because around $Re = 2000$, the intermittent structure is a pattern-structured turbulent stripe, which has robustness and no DP-like active splitting. It is suggested that all duct transitions with $A \gtrsim 96$ follow $(2+1)$-D DP, whereas $(1+1)$-D DP for not so high-aspect-ratio due to the formation of quasi-one-dimensional turbulent spots like the turbulent puff in the transitional pipe flow.

Table 2. Critical Reynolds number Re_c and the critical exponent β_{fit} expected by Equation (5) for each fitting range. Also shown is the global critical Reynolds number Re_g, which is the lower limit of the globally sustained turbulence, cited from Kohyama *et al.* (under review). For reference, the theoretical critical exponents β of the two types of DPs are listed below.

Case	Re_g	Re_c	β	Fitting range
$A24$	1105	1119	0.28 ± 0.02	1100–1600
$A96$	1058	999	0.57 ± 0.03	1100–1405
$A\infty$	722	994	0.58 ± 0.19	1155–1405
$(1+1)$-D DP	—	—	~ 0.276	—
$(2+1)$-D DP	—	—	~ 0.583	—

CONCLUSION

In the present study, directed percolation (DP) phenomena in the STIs of localized turbulence and there transition profiles on subcritical regime have been investigated in two high-aspect-ratios ($A = 24$ and 96) duct flows and the infinitely wide channel flow (PPF) by DNS to characterize its phenomenon. Since the structure and behavior of intermittency become larger near the criticality, the previous experimental and numerical studies have not yet been able to capture the essence of the critical phenomena due to insufficient domain and statistics. Long-term Lagrangian observations of the interaction of multiple localized turbulences were performed in the present DNSs for the largest-scale domain.

For the effects of the presence or absence of sidewalls and the distance between sidewalls (*i.e.*, duct flow or PPF, and aspect ratio) on the spatio-temporal intermittencies (STIs) and thus the transition profiles, the following points were found.

— The global turbulence maintenance limitation is approximately asymptotic to $Re_g = 1000$ even for high-aspect-ratio duct flows with spatial finiteness, as predicted on the experimental channel flow in Carlson *et al.* (1982). It does not maintain turbulence down to $Re_g = 722$ as in the PPF, and for $Re < 1000$ all turbulent spots and bands decay within a finite time, becoming fully-laminar flow.
— Local turbulence split and decay are significantly ob-

served in duct flow near the criticality ($Re \approx 1100$–1200), causing large-scale STI as a single series of branches. For medium aspect ratio ($A24$), turbulent spots and bands form quasi-one-dimensional intermittency only in the streamwise direction at the center of the sidewalls, closely similar to $(1+1)$-D DP branching. While, for high aspect ratio ($A96$), the intermittency is two-dimensional in the streamwise and spanwise directions, and the branching is close to $(2+1)$-D DP. However, near the sidewalls, localized turbulent is not actively splitting, but is often decaying, etc., and its branching has no DP-like features.

— The Reynolds number dependency of the turbulent fraction (transition profile) follows the scaling of the power law of DP around the critical value. The profiles of the duct flows with $A24$, and $A96$, and the PPF at $Re \approx 1100$ were consistent with the critical exponents of $(1+1)$-D and $(2+1)$-D DP universality classes, respectively.

For future work, a detailed discussion of DP universality classes would require a quantitative investigation of the critical exponents by power law scalings, not only for the transition profile, but also for the laminar gap distributions of the STI.

Present numerical simulations were performed on the SX-ACE and SX-Aurora TSUBASA supercomputers with technical support from the Cyberscience Center at Tohoku University. This work was funded by Grant-in-Aid for the JSPS (Japan Society for the Promotion of Science) Fellowships (grant number: JP19H02071 and JP22J14598). The first author (K.K.) expresses appreciation for the Fellowship Program for Material Science Researcher at Tokyo University of Science, which is supported by MEXT (the Ministry of Education, Culture, Sports, Science and Technology).

REFERENCES

Abe, H., Kawamura, H. & Matsuo, Y. 2001 Direct numerical simulation of a fully developed turbulent channel flow with respect to the Reynolds number dependence. *J. Fluids Eng.* **123** (2), 382–393.

Avila, K., Moxey, D., de Lozar, A., Avila, M., Barkley, D. & Hof, B. 2011 The onset of turbulence in pipe flow. *Science* **333** (6039), 192–196.

Barkley, D. & Tuckerman, L. S. 2005 Computational study of turbulent laminar patterns in Couette flow. *Physical Review Letters* **94** (1), 014502.

Carlson, D. R., Widnall, S. E. & Peeters, M. F. 1982 A flow-visualization study of transition in plane Poiseuille flow. *Journal of Fluid Mechanics* **121**, 487–505.

Chantry, M., Tuckerman, L. S. & Barkley, D. 2016 Turbulent-laminar patterns in shear flows without walls. *Journal of Fluid Mechanics* **791**, R8.

Duguet, Y., Schlatter, P. & Henningson, D. S. 2010 Formation of turbulent patterns near the onset of transition in plane Couette flow. *Journal of Fluid Mechanics* **650**, 119–129.

Fadlun, E., Verzicco, R., Orlandi, P. & Mohd-Yusof, J. 2000 Combined immersed-boundary finite-difference methods for three-dimensional complex flow simulations. *Journal of Computational Physics* **161** (1), 35–60.

Henkel, M., Hinrichsen, H. & Lübeck, S. 2008 *Non-Equilibrium Phase Transitions Volume I: Absorbing Phase Transitions*. Springer.

Kashyap, P. V., Duguet, Y. & Dauchot, O. 2020 Flow statistics in the patterning regime of plane channel flow. *Entropy* **22** (9), 1001.

Khan, H. H., Anwer, S. F., Hasan, N. & Sanghi, S. 2021 Laminar to turbulent transition in a finite length square duct subjected to inlet disturbance. *Physics of Fluids* **33**, 065128.

Klotz, L., Lemoult, G., Avila, K. & Hof, B. 2022 Phase transition to turbulence in spatially extended shear flows. *Physical Review Letters* **128**, 014502.

Kohyama, K., Sano, M. & Tsukahara, T. under review Sidewall effect on turbulent band in subcritical transition of high-aspect-ratio duct flow .

Lemoult, G., Aider, J.-L. & Wesfreid, J. E. 2012 Experimental scaling law for the subcritical transition to turbulence in plane Poiseuille flow. *Physical Review E* **85** (2), 025303.

Lemoult, G., Shi, L., Avila, K., Jalikop, S. V., Avila, M. & Hof, B. 2016 Directed percolation phase transition to sustained turbulence in Couette flow. *Nature Physics* **12** (3), 254–258.

Manneville, P. & Shimizu, M. 2020 Transitional channel flow: A minimal stochastic model. *Entropy* **22** (12), 1348.

Moin, P. & Kim, J. 1982 Numerical investigation of turbulent channel flow. *Journal of Fluid Mechanics* **118**, 341–377.

Mukund, V. & Hof, B. 2018 The critical point of the transition to turbulence in pipe flow. *Journal of Fluid Mechanics* **839**, 76–94.

Orszag, S. A. 1971 Accurate solution of the Orr–Sommerfeld stability equation. *Journal of Fluid Mechanics* **50** (4), 689–703.

Paranjape, C. S. 2019 Onset of turbulence in plane poiseuille flow. PhD thesis, IST Austria Klosterneuburg, Austria.

Pomeau, Y. 1986 Front motion, metastability and subcritical bifurcations in hydrodynamics. *Physica D: Nonlinear Phenomena* **23** (1-3), 3–11.

Prigent, A., Grégoire, G., Chaté, H., Dauchot, O. & van Saarloos, W. 2002 Large-scale finite-wavelength modulation within turbulent shear flows. *Physical Review Letters* **89** (1), 014501.

Sano, M. & Tamai, K. 2016 A universal transition to turbulence in channel flow. *Nature Physics* **12**, 249–253.

Seki, D. & Matsubara, M. 2012 Experimental investigation of relaminarizing and transitional channel flows. *Physics of Fluids* **24** (12), 124102.

Shimizu, M. & Manneville, P. 2019 Bifurcations to turbulence in transitional channel flow. *Physical Review Fluids* **4** (11), 113903.

Takeda, K., Duguet, Y. & Tsukahara, T. 2020 Intermittency and critical scaling in annular couette flow. *Entropy* **22** (9), 998.

Takeda, K. & Tsukahara, T. 2019 Subcritical transition of plane poiseuille flow as (2+1)d and (1+1)d dp universality classes. In *In Abstract Proceedings of the 8th Symposium on Bifurcations and Instabilities in Fluid Dynamics (BIFD2019)*.

Takeishi, K., Kawahara, G., Wakabayashi, H., Uhlmann, M. & Pinelli, A. 2015 Localized turbulence structures in transitional rectangular-duct flow. *Journal of Fluid Mechanics* **782**, 368–379.

Tao, J., Eckhardt, B. & Xiong, X. 2018 Extended localized structures and the onset of turbulence in channel flow. *Physical Review Fluids* **3** (1), 011902.

Tsukahara, T., Kawaguchi, Y., Kawamura, H., Tillmark, N. & Alfredsson, P. 2010 Turbulence stripe in transitional channel flow with/without system rotation. In *Proc. Seventh IUTAM Symp. on Laminar-Turbulent Transition* (ed. P. Schlatter & D.S. Henningson), pp. 421–426. Springer.

Tsukahara, T., Seki, Y., Kawamura, H. & Tochio, D. 2005 DNS of turbulent channel flow at very low Reynolds numbers. In *TSFP Digital Library Online*, pp. 935–940. Begel House Inc.

Tuckerman, L. S. & Barkley, D. 2011 Patterns and dynamics in transitional plane Couette flow. *Physics of Fluids* **23** (4), 041301.

Tuckerman, L. S., Chantry, M. & Barkley, D. 2020 Patterns in wall-bounded shear flows. *Annual Review of Fluid Mechanics* **52**, 343–367.

Wu, H. & Song, B. 2022 A numerical study of the side-wall effects on turbulent bands in channel flow at transitional Reynolds numbers. *Computers & Fluids* **240**, 105420.

Xiao, Y., Tao, J. & Zhang, L. 2021 Self-sustaining and propagating mechanism of localized wave packet in plane-Poiseuille flow. *Physics of Fluids* **33** (3), 031706.

Yimprasert, S., Kvick, M., Alfredsson, P. H. & Matsubara, M. 2021 Flow visualization and skin friction determination in transitional channel flow. *Experiments in Fluids* **62** (2), 1–16.